

Bidirectional Flyback based Isolated-port Submodule Differential Power Processing Optimizer for Photovoltaic Applications

Guanying Chu^a, Huiqing Wen^{a,*}, Lin Jiang^b, Yihua Hu^b, Xingshuo Li^a

^aDepartment of Electrical and Electronic Engineering, Xi'an Jiaotong-Liverpool University, Suzhou, China
Email: Huiqing.Wen@xjtlu.edu.cn, Tel: +86 (0)512 8188-0477, Fax: +86 (0)512 8188-0445

^bDepartment of Electrical Engineering and Electronics, University of Liverpool, Liverpool, L69 3GJ, United Kingdom

Abstract

Partial shading brings many serious problems in the solar photovoltaic system (SPV) such as the significant reduction in power harvest, hot spots, and the emergence of the multiple maximum power points (MPPs). This paper presents a bidirectional flyback converter (BFC) based isolated-port differential power processing (DPP) architecture at the submodule level. Bidirectional flyback converters (BFCs) are designed for submodules with both discontinuous condition mode (DCM) and continuous condition model (CCM) modes for light-load and heavy-load conditions to improve the efficiency. The voltage equalization with open-loop control is adopted for each BFC, this control method keeps the voltage in primary and secondary of the BFCs equal and it does not require additional voltage or current sensors. It's simple, easy-to-implement and well suited for low-cost integrated hardware scheme. Both simulation and experimental results for an isolated-port DPP regulated 72-cells photovoltaic (PV) module under various partial shading scenarios were provided. It shows that this structure can distinctly mitigate the energy loss in a PV system, increase output power harvest, and achieve high efficiency under partial shading condition. The measured efficiency with the isolated-port DPP structure was 90.23% under severe shading condition. The measured output power improvement under severe mismatch condition was high up to 43.1%.

Key words

Photovoltaic (PV) system, partial shading conditions, differential power processing, bidirectional flyback converters (BFCs).

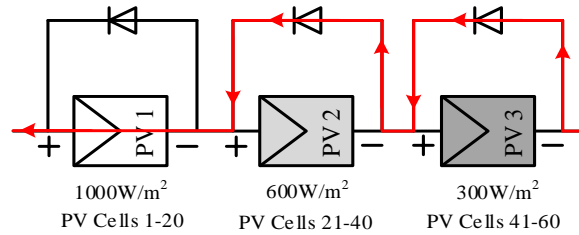
NOMENCLATURE

I_{string}	String level current
V_{module}	Module voltage
$I_{pri,i(i=1,2,3)}$	Primary current of bidirectional flyback converter
$I_{sec,i(i=1,2,3)}$	Secondary current of bidirectional flyback converter
$V_{sub,i(i=1,2,3)}$	Terminal voltage of submodule
V_{sec}	Secondary voltage of bidirectional flyback converter
$i_{g,i(i=1,2,3)}$	Output current of submodule
$V_{pri,i(i=1,2,3)}$	Primary voltage of bidirectional flyback converter
C_{pri}	Primary capacitor of bidirectional flyback converter
C_{sec}	Secondary capacitor of bidirectional flyback converter
Q_{pri}	Primary device of bidirectional flyback converter
Q_{sec}	Secondary device of bidirectional flyback converter
$P_{DPP,max}$	Maximum output power with DPP structure
$P_{MPPT,max}$	Ideal maximum output power
δ	Power loss percentage
N_s	Number of cells
V_{mpp}	Voltage at maximum power point (MPP)
V_{oc}	Open-circuit voltage
E_g	Band energy
R_p	Shunt resistance
P_{mpp}	Maximum power
I_{mpp}	Current at MPP
I_{sc}	Short-circuit current
R_s	Series resistance
P_{DPP}	System output power by using DPP
P_{MPPT}	System output power by using MPPT
SIM	Simulation
EXP	Experiment

I. INTRODUCTION

In the real world, photovoltaic (PV) panels are connected in series to form a string generating a high DC voltage, and then these strings are connected in parallel to create an array for building photovoltaic grid power generation system. The whole PV systems are presenting a high-power conversion efficiency but have been proved significantly reduced for output energy harvesting under non-ideal real-world conditions (Mäki and Valkealahti 2012). The loss is mainly caused by the mismatch among PV cells, which may be generated by

either external factors (partial shading, dust gathered, and angle differences) or internal factors such as manufacturing process and PV cells degradation (Bai, Cao et al. 2015, Mai, De Breucker et al. 2017, Lappalainen and Valkealahti 2017). The mismatch among PV cells will not only cause the loss of energy but also bring hotspot effects, which eventually affects the reliability and lifetime of PV modules. Bypass diodes are widely used to prevent the failures due to the hotspot. Typically, one bypass diode can protect one PV substring with 20-24 cells. However, the reduction of output power is also significant since the bypassed PV cell substring is unable to work properly and the string current is also affected by a small number of shaded PV cells (Kim, Seo et al. 2016, Daliento, Di Napoli et al. 2016). Fig. 1(a) illustrates the string current flow path of a PV module with three bypass diodes parallel-connected under mismatch conditions among the submodules, where submodules PV2 and PV3 are shaded with less insolation compared with PV1. With the conventional method, the module output power is affected due to partial shading, and subsequently, three peaks are observed in the power-voltage (P-V) curve, including a global maximum power point (GMPP) and multiple local maximum power points (LMPPs), as shown in Fig. 1(b). Classical MPPT techniques such as incremental conductance (Radjai, Rahmani et al. 2014, Tey and Mekhilef 2014), beta method (Li, Wen et al. 2016) and perturbation & observe (P&O) (Rezk and Eltamaly 2015) are unable differentiate the GMPP and LMPPs. Furthermore, the bypassed PV cells cannot output power properly, which could not be recovered by the GMPP tracking (GMPPT) algorithms.



(a)

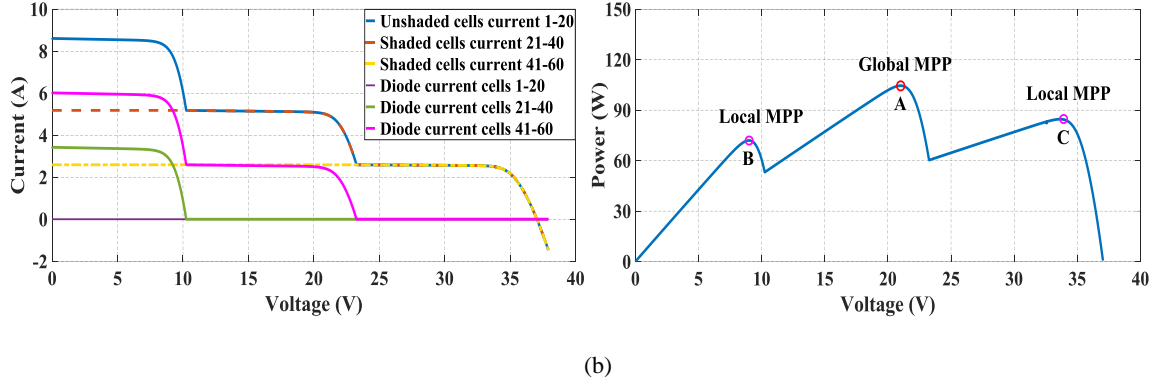


Fig. 1. PV module under partial shading condition: (a) string current flow path and (b) the characteristics of I-V and P-V curves

Some new architecture such as DC power optimizers (DCPO) and differential power processing (DPP) are proposed to solve these issues (Du and Lu 2011, Solórzano and Egidio 2014, Khan and Xiao 2016, Khan and Xiao 2017). DCPO is PV-panel-level converters, connected in a cascaded architecture to keep each panel working on its MPP to mitigate the mismatch. In DCPO architecture as shown in Fig. 2(a), the converters are required to process the full power generated by each PV panel that the architecture efficiency depends on the effectiveness of the converter. Differential power processing (DPP) architecture is proposed to solve the submodule-level mismatch problem, which provides a way to overcome mismatch problem among PV modules by enabling each PV element connected in a series string to work on its MPP. More specific introduction to the DPP concept in photovoltaic application can be found in (Shenoy, Kim et al. 2013). Compare with DCPO, the DC-DC converters in DPP architecture only need to process the differential power caused by partial shading or others mismatch conditions (Kim, Shenoy et al. 2015, Qin, Barth et al. 2016, Khan and Xiao 2017). Since this part of differential power accounts for only a small part of total output power and most of the power is flowing into the modules, DPP can substantially improve the system efficiency and reduce the cost of hardware, which is a major advantage of the DPP architecture. When the mismatch doesn't exist, DPP converters can be regulated to the off state, and there is no power loss. Furthermore, different from the DCPO, the efficiency of DPP converter has an insignificant effect on the entire system. Thus, the design flexibility is improved.

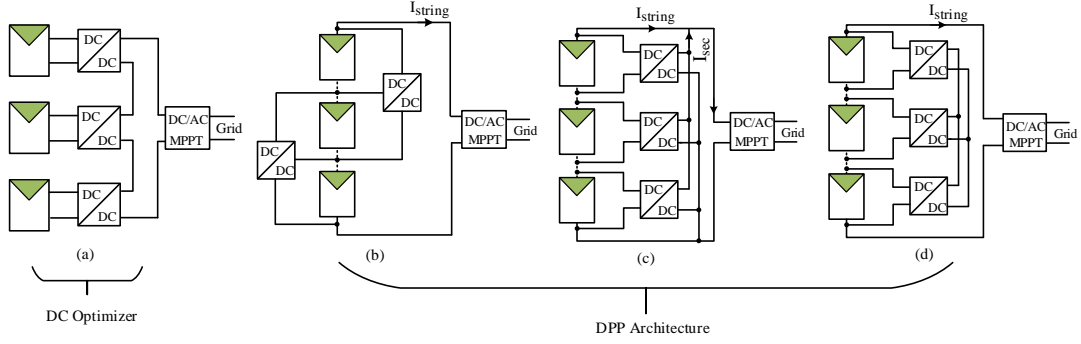


Fig.2. (a) DC optimizer architecture, (b) PV-PV DPP architecture, (c) PV-to-non-isolated port bus DPP architecture, (d) PV-to-isolated port bus DPP architecture.

Basically, the DPP architectures are mainly divided into three categories with different connection: PV-PV as shown in Fig. 2(b), PV-to-non-isolated port bus (PV-to-NIP) as shown in Fig. 2(c), and PV-to-Isolated Port (PV-to-IP) as shown in Fig. 2(d). The number of DC-DC converters in the PV-PV architecture is always one less than that of PV modules (Shenoy, Kim et al. 2013, Khan and Xiao 2017). Communication among each adjacent DC-DC converter is generally required to implement the MPPT algorithm, which adds system cost and complexity (Khan and Xiao 2017). As illustrated in Fig. 2(c) and Fig. 2 (d), the difference between PV-to-NIP and PV-to-IP architecture lies in whether the current in secondary of DC-DC converters flows into the string level circuit. In the PV-to-NIP architecture, the secondary side of the DPP converters is connected in parallel and share a same DC-link voltage with the central inverter for grid connection. Since the DC-link voltage is the sum of the PV module output voltage, the devices for the secondary-side switches of module-level DC-DC converter need to withstand the high voltage stress, which increases the power loss and cost. Besides, the communication between module-level converters and the central inverter is also required for the MPPT control (Olalla, Clement et al. 2013, Khan and Xiao 2017). The diagram for the PV-to-IP architecture is shown in Fig. 2(d). Since the secondary ports of DC-DC converters are connected in parallel to form an isolated port, the port voltage can be selected independently from the PV module voltage, which shows high design flexibility in terms of minimizing the size and power loss of module-level converters. The voltage equalization control is also easily implemented without communication circuits between DC-DC converters and the central inverter. Furthermore, a simple filter can be used in the isolated port, which is beneficial the system cost and efficiency (Olalla, Clement et al. 2013).

DC-DC converters are a key design aspect of DPP system and have been discussed, named as PV balancer

(Zhou, Zhao et al. 2015), PV equalizers (Ben-Yaakov, Blumenfeld et al. 2012, Villa, Ho et al. 2013) . Main topologies include bidirectional buck-boost converters (Qin, Cady et al. 2015, Qin, Barth et al. 2016), multi-stacked buck boost converters (Uno and Kukita 2015), switched capacitor (Schaefer, Kesarwani et al. 2013), and BFCs (Olalla, Clement et al. 2013, Shenoy, Kim et al. 2013, Bell and Pilawa-Podgurski 2015, Kim, Shenoy et al. 2015). In this paper, bidirectional flyback topology is finally selected since it can achieve voltage isolation, high efficiency for a wide range, and easy gate driver circuit design.

Control for the submodule DC-DC converters in various DPP structures is also challenging. Basically, two categories methods can be used: true MPPT control and voltage equalization. True MPPT control achieves the theoretical maximum output power for each submodule. However, the control is relatively complicated. Voltage equalization, also referred to voltage balancing in (Levron, Clement et al. 2014), is regarded as a sub-optimal MPPT method, it is not a true MPPT but equalized voltage of each submodule at a point close to its MPP. In (Levron, Clement et al. 2014), a closed-loop control method was discussed to achieve voltage equalization with the architecture of PV-to-isolated port. A 96% efficiency under significant partial shading was achieved, as illustrated by the experiment results. In (Qin, Barth et al. 2016), a bidirectional buck-boost converter was used in PV-to-PV architectures with fixed duty ratio control to achieve voltage equalization. Both (Qin, Cady et al. 2015) and (Uno and Kukita 2015) discussed DPP based PV system without local current sensors. In (Qin, Cady et al. 2015), a true MPPT method related to a distributed P&O algorithm was used. In (Uno and Kukita 2015), the voltage equalization was used, and the topology was multi-stacked buck-boost converters.

In this paper, the PV-to-IP DPP architecture is selected with the bidirectional flyback converter (BFC) topology selected as the submodule integrated converter. The voltage conversion ratio of flyback converters is easily adjusted by changing the turn ratio of the transformer. Furthermore, both discontinuous condition mode (DCM) and continuous condition model (CCM) are implemented for the flyback converters (Eng and Bunlaksananusorn 2009, Eng, Pinsopon et al. 2009). Specifically, to improve the converter efficiency, CCM and DCM are implemented for the severe and light shading conditions, respectively. This paper takes three substrings and three submodule integrated converters as an example. In fact, the architecture can be extended to any number of submodules, where all BFCs share the same isolated secondary port. The BFCs are controlled by voltage equalization with an open-loop control. Specifically, the DPP converters work with a

fixed 0.5 duty-cycle when PV submodules are arranged under mismatch conditions. No additional voltage or current sensors are required. Complex processing and communication between BFCs are also removed. Both simulation and experimental tests under various scenarios have been carried out to evaluate the performance of the flyback-based isolated-port DPP structure.

II. SYSTEM ARCHITECTURE

A. DPP architecture in this paper

Fig. 3 shows the schematic diagram of the proposed DPP architecture, consisting of three submodules in one PV module, specifically it is a 72-cells module that includes 3 sub-modules and each sub-module consists of 24-cells. The converters in DPP system are connected in parallel and share a common isolated-port so that that the voltage on the secondary side of each converter is equal.

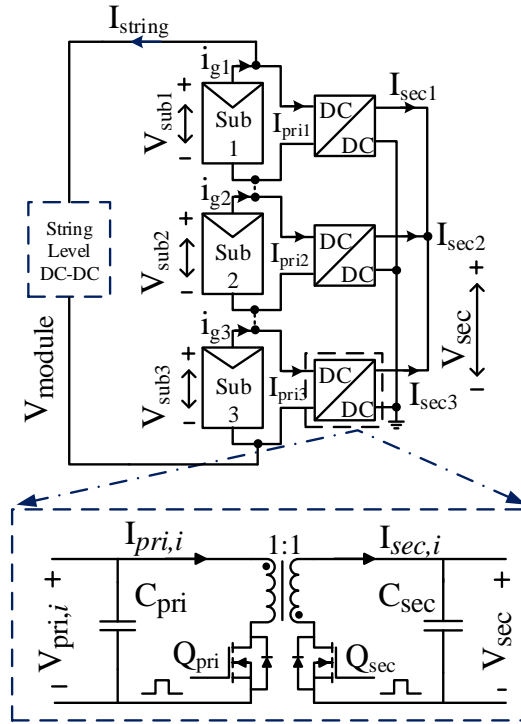


Fig. 3. Isolated-port DPP architecture with bidirectional flyback converters

In this design, the converter topology is finally selected as the BFC considering the requirements for voltage isolation, efficiency, and design difficulty, especially for the gate driver circuits. With proper control strategies, each DPP converter outputs a regulated voltage with respect to those of adjacent submodules. Furthermore, it can adjust the output power of each submodule close to its maximum individual power.

Majority current flows directly through the load, and a small fraction of the differential current is processed by the DPP converter. In this paper, the PV-20 SFP2136 is selected as the PV module, and its main electrical specifications under the STC are presented in Table I.

TABLE I
PV MODULE SPECIFICATION (PV-20 SFP2136)

Parameter	Symbol	Value	Parameter	Symbol	Value
Number of cells	N_s	24	Maximum power (W)	P_{mpp}	20
Voltage at MPP (V)	V_{mpp}	17.2	Current at MPP (A)	I_{mpp}	1.11
Open-circuit voltage (V)	V_{oc}	21.6	Short-circuit current (A)	I_{sc}	1.22
Temperature coeff. Of V_{oc} (%/°C)	NA	-0.034	Temperature coeff. Of I_{sc} (%/°C)	NA	0.005
Band energy (eV)	E_g	1.12	Ideality factor	NA	1.8
Shunt resistance (Ω)	R_p	25	Series resistance (Ω)	R_s	0.008

B. Control Algorithm

The main objective of the BFCs is to balance the voltage of the submodules, which is called here voltage equalization. The aim of this control strategy is to keep the voltage in primary and secondary of the DPP converters same. Specifically, a fixed 50% duty cycle signal is used to control the switches in DPP converter. The input voltage V_{pri} , output voltage V_{sec} and duty cycle D in flyback converter have the relation as follows:

$$V_{sec} = V_{pri} \frac{D}{1-D} \quad (1)$$

Furthermore, the secondary sides of the BFCs are connected in parallel. Thus, the output voltage is equal. Then the equation can be written as follows:

$$\begin{aligned} V_{sec} &= V_{pri_1} \frac{D}{1-D} \\ V_{sec} &= V_{pri_2} \frac{D}{1-D} \\ V_{sec} &= V_{pri_3} \frac{D}{1-D} \end{aligned} \quad (2)$$

where V_{pri_1} , V_{pri_2} and V_{pri_3} is the voltage of each substring. Let D is equal to 0.5, then $V_{sec} = V_{pri_1} = V_{pri_2} = V_{pri_3}$. Therefore, the voltage of each substring is controlled to reside on a straight line. Fig. 4 illustrates the operation principle of the submodule flyback converters in DPP architecture to balance the voltage. To transfer the energy from primary to secondary of BFCs, switch Q_{pri} is controlled by conventional constant-frequency pulse-width modulation, and the duty cycle is calculated as $D=T_{on}/T_s$, where T_{on} is the

switch on time, and T_s is the switching period. Meanwhile, the switch Q_{sec} in the secondary side of BFC is shut off at all time, and the built-in diode is worked as the flyback diode. If the energy transfer direction is reversed, the operation of the converters is complete symmetrical: Q_{pri} in primary side is turned off at all time while its built-in diode acts as the flyback converter, meanwhile, switch Q_{sec} is now controlled by PWM pulses. C_{pri} and C_{sec} represent the primary side and secondary side capacitor, respectively.

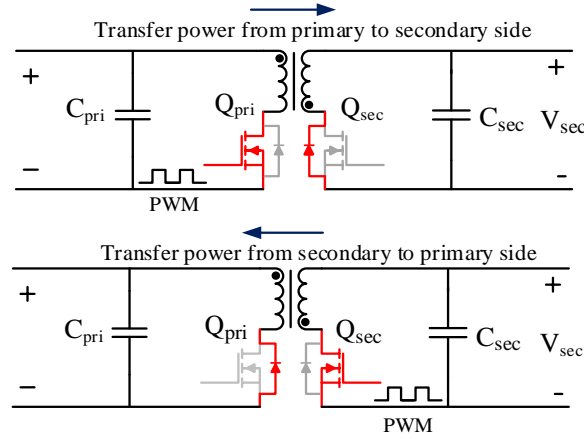


Fig. 4. The operation principle of flyback converters in DPP architecture to balance the voltage.

In this paper, voltage equalization, a simple and robust method, is used with no communication or sensing between primary and secondary of the flyback converter. A complementary signal with frequency 100 kHz and 0.5 duty ratio are used to control the primary switch Q_{pri} and secondary switch Q_{sec} according to the power transfer direction. A comparison of the voltage equalization and true MPPT is made in the following section; it shows that this control method simplifies the system configuration and reduces the cost of hardware.

III. PERFORMANCE EVALUATION

A. Comparison between DPP and bypass diode method

The limitation of the conventional bypass diode method is that the actual output power is significantly reduced and the output P-V curve shows multi-peaks characteristic under partial shading conditions. Here, a comparison between the proposed DPP structure and the method of using bypass diodes under different partial shading scenarios is conducted. Specifically, the following three scenarios are defined: severe mismatch condition with PV1 fully illuminated, PV2 half illuminated, and PV3 25% illuminated; moderate mismatch condition with the normalized illumination values for these three submodules 100%, 75%, and 50%; slight mismatch condition, the normalized illumination values for these submodules are 100%, 90%,

and 80%. As illustrated in Fig. 5(a) and (b), under the slight mismatch condition, the reduction of output power produced by the bypass diode method is not distinct, and the improvement with the proposed DPP is small, specifically 5.32%. It shows that PV module will operate at near the theoretical maximum power output point and the power proceeded by the BFCs is very small. However, with the increase of partial shading area, the improvement with the DPP becomes larger, specifically 33.91% for moderate partial shading condition and 56.25% for serious partial shading condition. Under these two scenarios, the module current I_{module} mainly limited by the weakest submodule and a large portion of the power produced by the strongest submodule cannot be used without DPP converters.

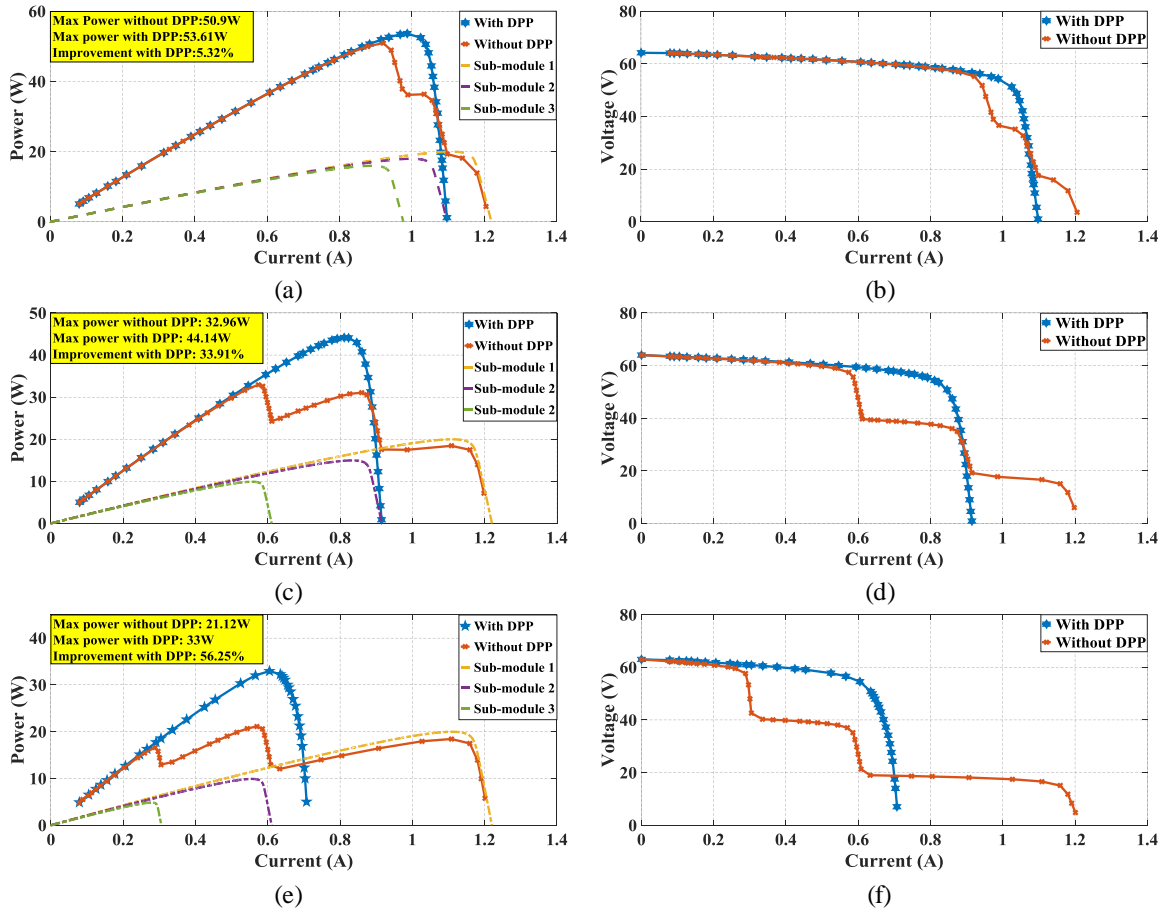


Fig. 5. Simulation results comparison: (a) P-I curve for slight mismatch condition (PV1: 100%, PV2: 90%, PV3: 80%); (b) V-I curve for slight mismatch condition (PV1: 100%, PV2: 90%, PV3: 80%); (c) P-I curve for moderate mismatch condition (PV1: 100%, PV2: 75%, PV3: 50%); (d) V-I curve for moderate mismatch condition (PV1: 100%, PV2: 75%, PV3: 50%); (e) P-I curve for severe mismatch condition (PV1: 100%, PV2: 50%, PV3: 25%); (f) V-I curve for severe mismatch condition (PV1: 100%, PV2: 50%, PV3: 25%).

Fig. 6 illustrates the difference of maximum output power between DPP and the bypass diode method in all irradiance conditions. In this test, the normalized insolation of the submodule 1 is always set to 100%.

The normalized insolation of sub-module 2 is set to 25%, 50%, 75% and 100%, and the normalized insolation of sub-module 3 is swept from 10% to 100%. Fig. 6 shows that the output power improvement is high up to 86% for the mismatch condition of PV1:100%, PV2: 25%, and PV3: 40%. As can be seen, a significant output power improvement can be achieved using DPP architecture, especially when the partial shading becomes more severe. In the moderate or severe partial shading scenarios, the string current is limited by the weakest submodules so that a significant portion of energy cannot be output for the system without DPP technology. The improvement of the maximum production power is not apparent when the mismatch among each submodule is slight. In these scenarios, each submodule typically works near the theoretical maximum output power, most of the energy flows directly into the string level control converters since the DPP converters only need to process very little power.

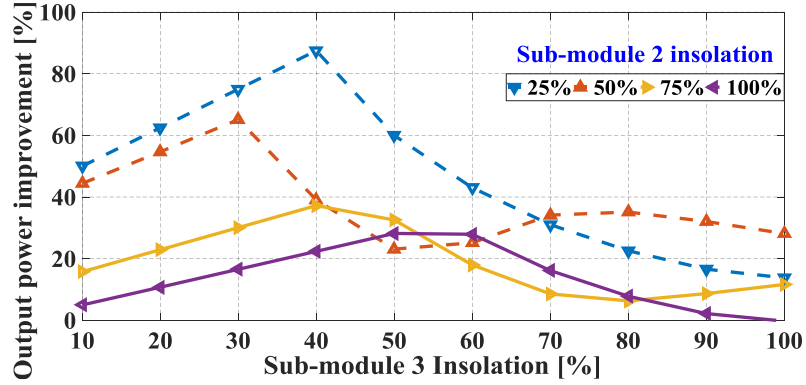


Fig. 6. Output power improvement under various insolation conditions

B. Comparison between True MPPT and voltage Equalization

Voltage equalization is used here since it doesn't require additional voltage or current sensors. Furthermore, the complex processing and communication between BFCs can also be removed. Thus, it's well suited for low-cost integrated hardware scheme. The basic principle of voltage equalization is to keep the voltage of each substring at the same straight line. However, it cannot ensure the operation point is the exact maximum power point because the MPP voltage for one PV panel is always changing with the temperature and irradiance as shown in Fig. 7. Nevertheless, when the mismatch between each submodule is not severe, the MPP voltage of each substring is nearly same.

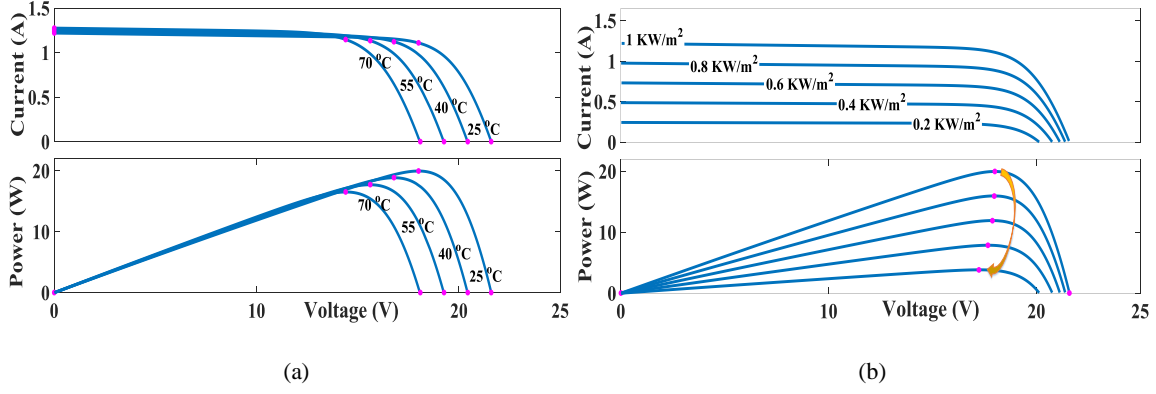


Fig. 7. (a) Solar P-V and I-V curve with variation in temperature at constant irradiance (1 kW/m^2), (b) solar P-V and I-V curve with variation in irradiance at constant temperature (25°C).

The following simulation has been tested in Matlab/Simulink to quantify the difference between true MPPT and voltage equalization, and the model is presented Fig. 8. A fixed-step P&O MPPT algorithm is used in this test. PV 1 is fixed at 100% normalized irradiance, PV 2 is fixed at 50% normalized irradiance and PV 3 is fixed at 25% normalized irradiance. The specifications of these three insolation conditions for PV-20 SFP2136 are listed in Table. II. The load used in this test is 40Ω . The output power and voltage of each PV panel for true MPPT and voltage equalization are observed.

TABLE. II
SPECIFICATION OF PV-20 SFP2136 WITH DIFFERENT IRRADIANCE

Irradiance	MPP Voltage	MPP Current	Maximum Power
1000 W/m^2	18 V	1.11 A	19.98 W
500 W/m^2	17.8 V	0.556 A	9.9 W
250 W/m^2	17.41 V	0.278 A	4.845 W

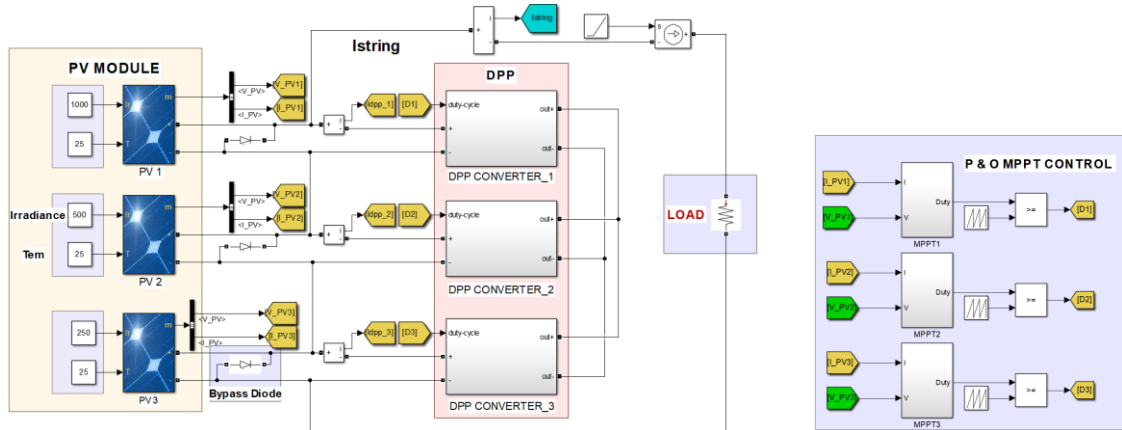


Fig. 8. Simulation model of the DPP module.

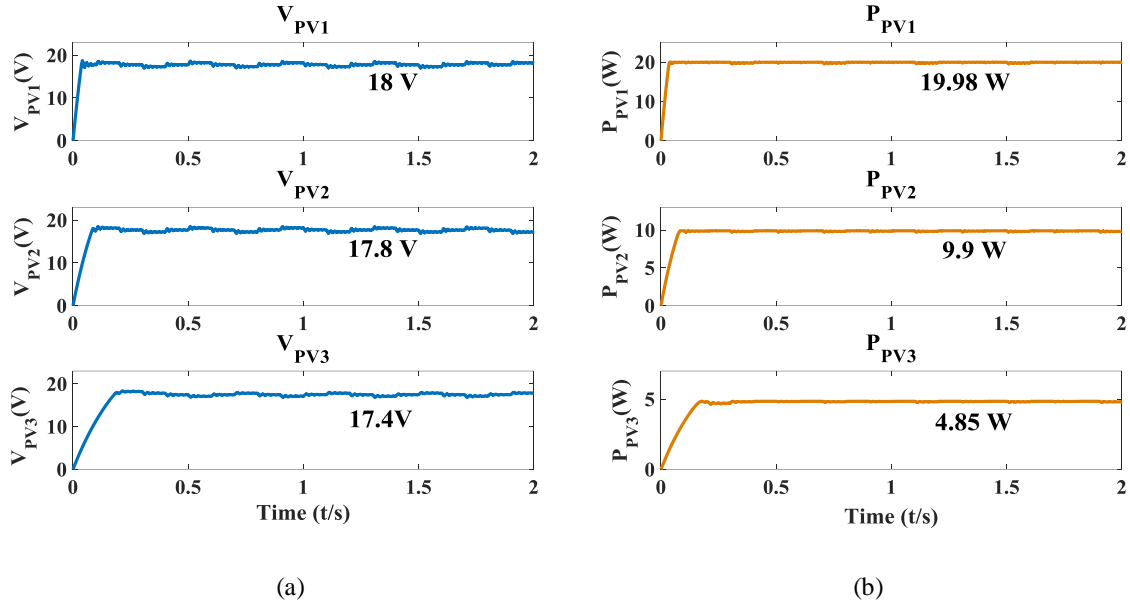


Fig. 9. Voltage waveform, power waveform and duty cycle of each substring by using true MPPT control method: (a) output voltage; (b) output power.

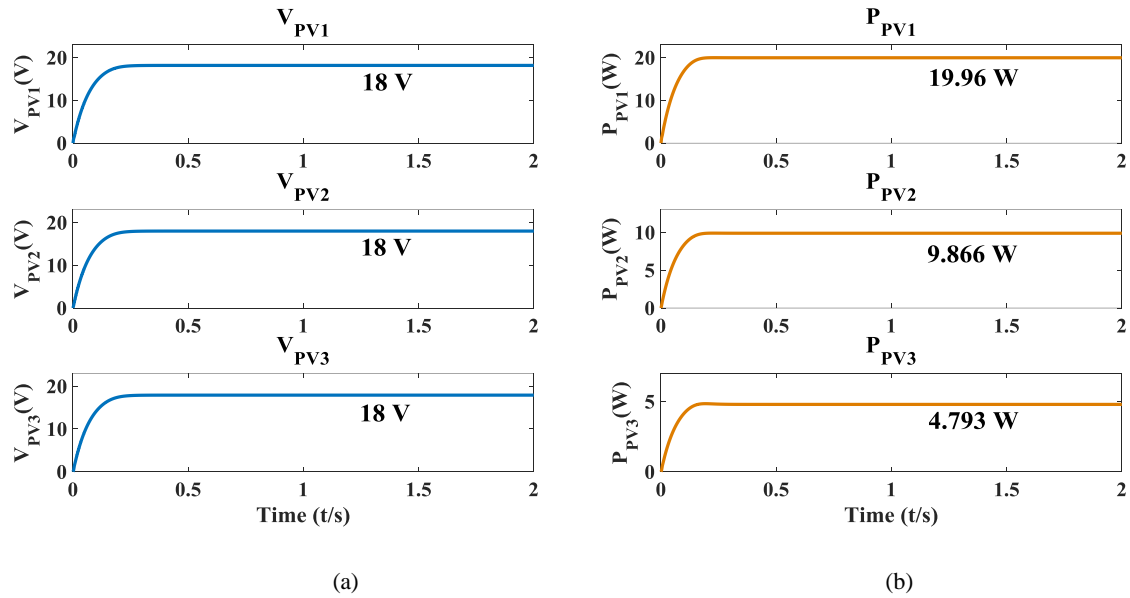


Fig. 10. Simulation results of each substring by using the voltage equalization method: (a) voltage waveform, (b) power waveform.

Fig. 9 presents the voltage waveform, power waveform and duty cycle of each substring by using true MPPT control. Fig. 10 presents the voltage waveform and power waveform by using method presented in this paper. The total output power with the true MPPT method is 34.73W, while the total output power of the voltage equalization method is 34.639 W with high efficiency of 99.73 %. The results can be summarized in

Fig.11. As can be seen, although voltage equalization is not a true MPPT, the voltage of operating points for each substring is nearly close to its ideal voltage of MPPs. While the DPP converters will balance the substring voltage, they cannot control the total output voltage V_{module} , which determines the total output power. External MPPT is used to adjust the V_{module} to search for the maximal power point. Thus, the whole control algorithm can be summarized as follows: the internal DPP converters direct to equalize the voltage of each substring that ensuring the operating point is on a straight line (the green line in Fig. 11). Then the external MPPT module is in charge of moving this line to ensure output power is maximal. The external MPPT algorithm is implemented according to the output P-V curve of the module and totally independently from the submodule integrated converter. Thus, the conventional MPPT algorithms can be selected for the external MPPT control.

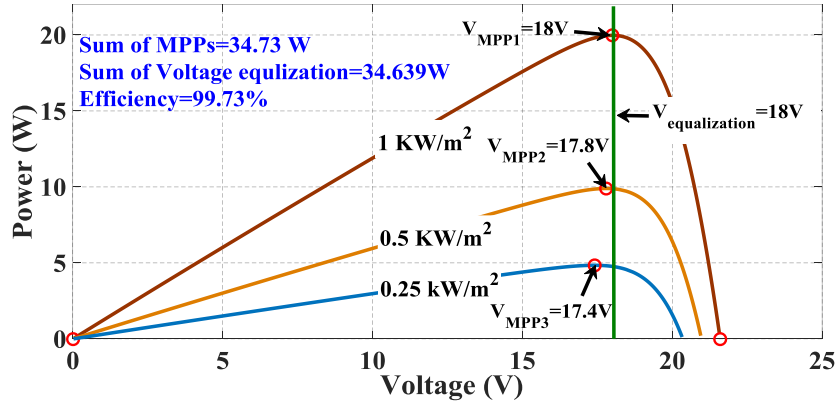


Fig. 11. P-V curve of each substring with insolation 1 KW/m², 0.5 KW/m², 0.25 KW/m².

A simulation is made under various mismatch conditions to quantify the difference of maximum output power between true MPPT and voltage equalization. In this test, the normalized insolation of the submodule 1 is fixed at 100%. The normalized insolation of submodule 2 is set to 25%, 50%, 75% and 100%, and the normalized insolation of submodule 3 is swept from 0 to 100%. Fig. 12 illustrates the obtained percentage power loss due to voltage equalization, which is defined as

$$\delta = 1 - \frac{P_{DPP,max}}{P_{MPPT,max}} \quad (3)$$

Fig. 12 shows that the obtained percentage power reduction due to voltage equalization is always kept less than 5.1% under various mismatch conditions. The maximum difference occurs for the condition of PV1:100%, PV2: 25%, and PV3: 10%. As illustrated by Fig. 12, the majority percentage of the output power reduction is less than 3%, which shows that the output power with the voltage equalization is very close to

the ideal maximum output power by using the complicated MPPT control for each submodule integrated converter. However, voltage equalization significantly reduces the control complexity since it can operate with open-loop control simply without real-time communication. Compared with true MPPT algorithm, the module current I_{module} doesn't be measured, which reduces the system cost. Furthermore, the proposed DPP can achieve satisfactory tracking efficiency. Consider the fact; the severe mismatch doesn't frequently occur in real-world installations. Thus, the voltage equalization is a satisfactory solution for the practical application.

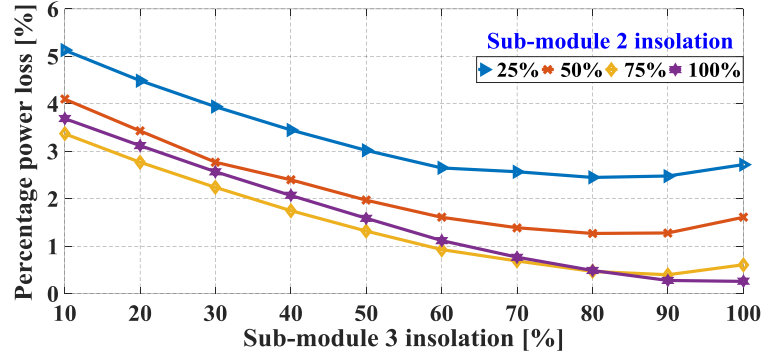


Fig. 12. Percentage power loss due to voltage equalization

C. Transient

Fig. 13 shows simulation results of the primary currents of each sub-module under dynamics. The electronic load of the whole system is 40Ω . In this simulation, all submodules are supplied with a same current 1.22A (meaning they have the same insolation level without any mismatch) at $t=0$. Then, at $t=0.4s$, the supplied current of submodule 2 becomes to 0.47A to emulate the mismatch condition. The primary theoretical current of DPP converters can be calculated by using following equation:

$$\begin{aligned}
 i_{pri1} &= i_{g1} - \frac{i_{g1} + i_{g2} + i_{g3}}{3} \\
 i_{pri2} &= i_{g2} - \frac{i_{g1} + i_{g2} + i_{g3}}{3} \\
 i_{pri3} &= i_{g3} - \frac{i_{g1} + i_{g2} + i_{g3}}{3}
 \end{aligned} \tag{4}$$

It should be noted that the sum of the primary current of all BFCs is zero that can be written as $I_{pri1} + I_{pri2} + I_{pri3} = 0$. Thus, the submodule 1 and submodule 3 eject currents and the mismatched submodule 2 extracts the current from others submodules.

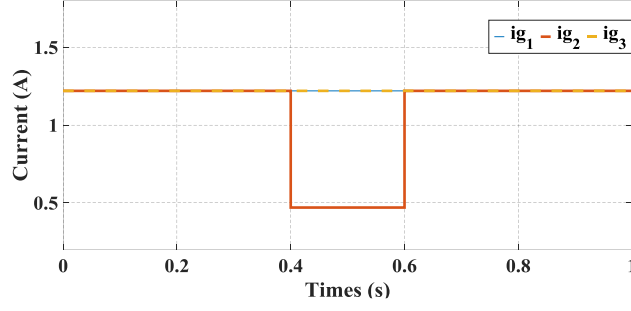


Fig. 13. The simulated current of each submodule during the mismatch transient.

The detailed dynamic waveforms during the time from 0.4s to 0.6s are illustrated in Fig. 14. The current of I_{pri1} and I_{pri3} are 0.25A and I_{pri2} is -0.5A under the mismatch condition. At $t=0.6$ s, the current of submodule 2 recovers to 1.22A and the BFCs stop extracting and ejecting currents. All primary currents of BFCs return to zero. The process can be illustrated specifically in Fig. 15.

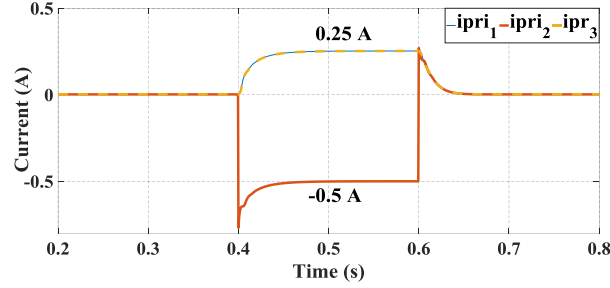


Fig. 14. Detailed primary current transient in each submodule.

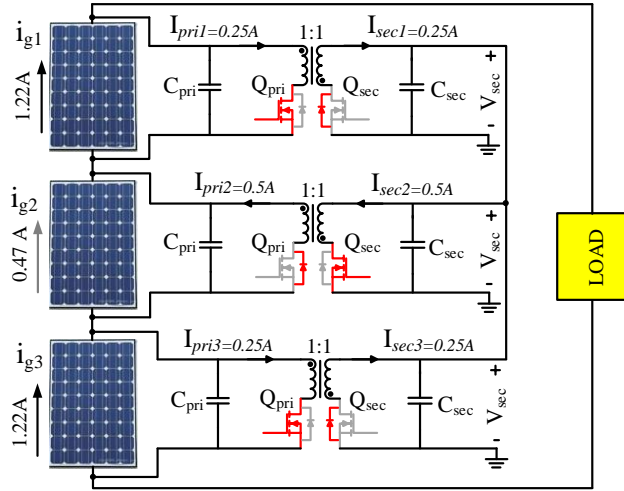


Fig. 15. The current following of each submodule flyback converter under partial shading.

IV. EXPERIMENTAL RESULTS

A. Experimental Setup

The system diagram of the experimental test setup and the detailed test bench arrangement are illustrated in Fig. 16 and Fig. 17, respectively. In the test, a 72-cells module was used, which can be separated into 3 sub-modules and each sub-module consists of 24 cells. In the test, considering the convenience in wire connecting, each sub-module was implemented by a 24-cells module. In this configuration, current source I_{phi} ($i=1, 2, 3$) is used to emulate the partial shading in three sub-modules. Practically the photo-diode I_{ph} for each sub-module is implemented by a DC power supply connected in parallel with each submodule and operated in current-limited mode. Different level of insolation can be easily accomplished by changing the value of I_{ph} . Thus, thus different partial shading conditions can be emulated. This indoor test was adopted considering its advantage of easy implementation and the repeatability.

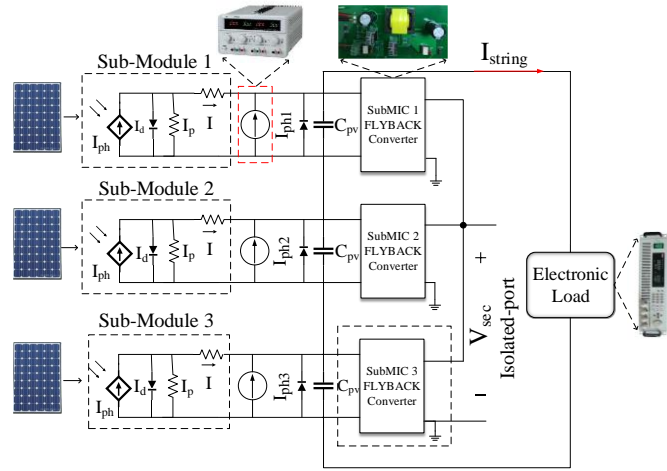


Fig. 16. Experimental test setup

The detailed test bench arrangement of the experiment is illustrated in Fig. 17. A prototype system has been built around PV-20 SFP2136 PV module with three BFCs attached three 24-cell substrings. Bias current source using in this paper is LK3303D connecting parallel with each submodule to emulate varying irradiation levels. DSP model TMS320F28335 is utilized in this experiment connecting with the computer to generate three sets of complementary signals input to the MOSFETs IRF740 in BFCs. Signal channel DC electronic load IT8514C+ used here to emulated external MPPT to control output module voltage V_{module} . Voltage probe DP6130A and connecting with the voltage and current probes to read the waveforms.

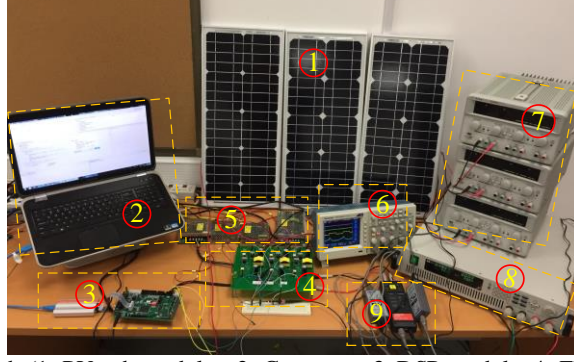


Fig. 17. Experimental test bench (1: PV sub-modules, 2: Computer, 3: DSP module, 4: Flyback converters, 5: Driving power supply, 6: Oscilloscope, 7: Bias Current Source, 8: Electronic Load, 9: Voltage and current probes)

Since the bidirectional flyback converters (BFCs) used in the DPP architecture process only the mismatch power of the PV submodules, which leads to reduced size, weight, and cost of the BFCs. Furthermore, the voltage rating of switching devices is reduced, which is same as the output voltage of each sub-module. Besides, the BFCs are only activated when partial shading is detected, which is also beneficial to the power loss reduction.

Two possible failure cases are considered: one case is that the primary or secondary port of one BFC operated under the open-circuit condition, the other case is the short-circuit condition in the secondary port of one submodule. For the former case, the actual output power is less power than that of MPP. However, due to the inside bypass diode of this submodule, the submodule still operates normally, and the output power reduction is relieved to some extent under mismatch conditions. For the latter case, it is usually regarded as the worst case, and thus all BFCs must be disabled to protect the entire system.

B. Bidirectional Flyback Converter Design and Test

To evaluate the effectiveness of the BFC based DPP architecture for PV system application, a real BFC prototype was designed and illustrated in Fig. 18.

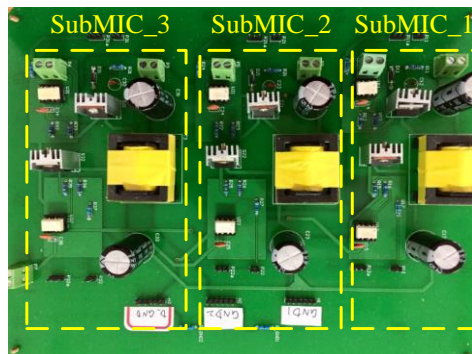


Fig. 18. Hardware prototype of the bidirectional flyback converter

When one 20W sub-module is fully illuminated, and the other two are completely shaded, the mismatch power is estimated around 13.3W. Thus, the power rating of the BFC was set as 15W. The switching device was selected as IRF740 and the switching frequency is 100 kHz. The transformer was designed with 10 turns of 18# Litz wire on the primary and secondary. The transformer was designed with 10 turns of 18# Litz wire on the primary and secondary. Litz wire is widely used in high-frequency transformer design since it can reduce the skin effect and proximity effect losses in conductors for high frequency applications. The magnetic inductance was $50\mu\text{H}$ and the leakage inductance was designed nearly 230nH . A snubber circuit with a diode and a 47pF capacitor was used to protect the main device MOSFET. The specific values of BFC are shown in Table III.

TABLE III
FLYBACK CONVERTER SPECIFICATION

Parameter	Value
Input voltage	4-21V
Flyback converter switching frequency	100kHz
Primary and secondary flyback converter switch	IRF740
Flyback converter turn ratio	1:1
Magnetizing inductance	$50\mu\text{H}$
Power Rating	15W
Primary and secondary capacitor	$2200\mu\text{H}$

An experimental test of the conversion efficiencies for the BFC was conducted and Fig. 19 shows key waveforms of the BFC with a constant duty cycle of 0.5 under different operating conditions. Fig. 19(a) illustrates the key waveforms of BFC under the slight partial shading condition, which indicates that the converter is working in discontinuous conduction mode (DCM). Fig. 19 (b) illustrates the key waveforms of BFC under the severe partial shading condition, which indicates that the converter is working in continuous conduction mode (CCM). Thus, different operation modes are used to improve the efficiency. Fig. 20 shows the measured efficiency of the BFC with respect to the output power, which indicates that the design BFC can achieve efficiency higher than 90% of a wide range of output power.

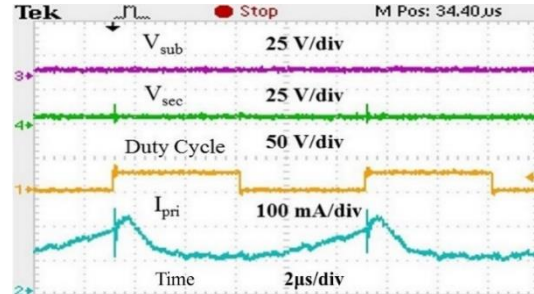
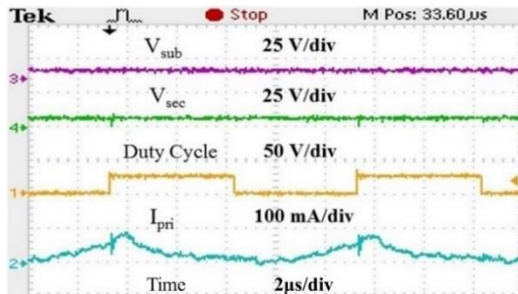


Fig. 19. Experimental waveforms of BFCs for two operating conditions: (a) slight partial shading condition; (b) severe partial shading condition.

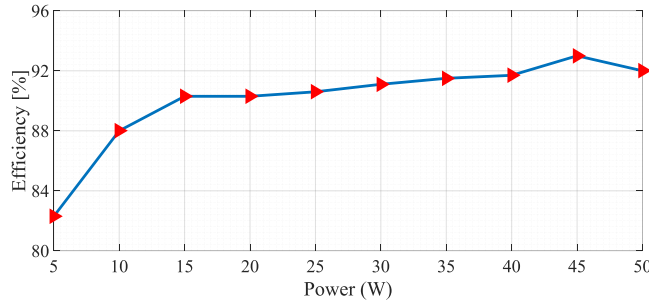


Fig. 20. Experimental efficiency for the bidirectional flyback converter with respect to the output power

C. Indoor Test

The experimental test setup is illustrated in Fig. 16. Main experimental setup was described in the section A. An electronic load, IT5814C+, is used as a central converter. Five multimeters are used to measure the voltage of each submodule; besides, the module-level voltage and current are also measured. In the indoor test, the short-circuit currents of the three sub-modules are tuned from 0A to 1.22A to emulate different partial shading conditions. To evaluate the performance of this BFC based DPP architecture, both the P-I and V-I curves with and without DPP algorithm are measured. As illustrated by Fig. 17, the electronic load is connected with the submodules and swept from 10Ω to 200Ω within 60 steps to perform a dc voltage sweep in order to characterize the P-I and V-I curves of the PV module. Fig. 21 illustrates main experimental results under three partial shading conditions. The definitions for three scenarios are the same as the simulation. Table IV also lists the comparison results of output power under different scenarios. As illustrated in Fig. 21 (a) and (b), under the slight mismatch condition, the P-I curves and V-I curves obtained from simulation and experiments are also overlapped since the BFCs only process a very small portion power. Under this scenario, as illustrated in Table IV, the improvement with the DPP structure through simulation and experiments is 5.32% and 3%, respectively. Considering the practical power loss of BFCs, the measured power improvement by experiment is lower than that of simulation. As illustrated in Fig. 21 (c) and (d), under the moderate mismatch condition, the difference of P-I curves and V-I curves obtained from simulation and experiments becomes larger. Under this scenario, the improvement with the DPP structure through simulation and experiments is 33.91% and 26%, respectively. Under the severe mismatch conditions, as illustrated in Table IV, the improvement with the DPP structure through simulation and experiments is 56.25% and 43.13%,

respectively. Consider the power loss in DPP converters during the test, the maximum power measured in the experiment is less than simulation. Furthermore, this error becomes more apparent when the mismatch level become severe because of more power loss in DPP converters in the experiment.

TABLE IV
EXPERIMENTAL RESULTS OF OUTPUT POWER UNDER DIFFERENT SCENARIOS

Mismatch Level	Slight	Moderate	Severe
Maximum power with DPP (SIM Results)	53.61 W	44.14 W	32.95 W
Maximum power with DPP (EXP Results)	52.29 W	41.5 W	30.23 W
Maximum power with Bypass Diodes	50.9 W	32.96 W	21.12 W
Improvement with DPP in SIM	5.32%	33.91%	56.25%
Improvement with DPP in EXP	3%	26%	43.13%

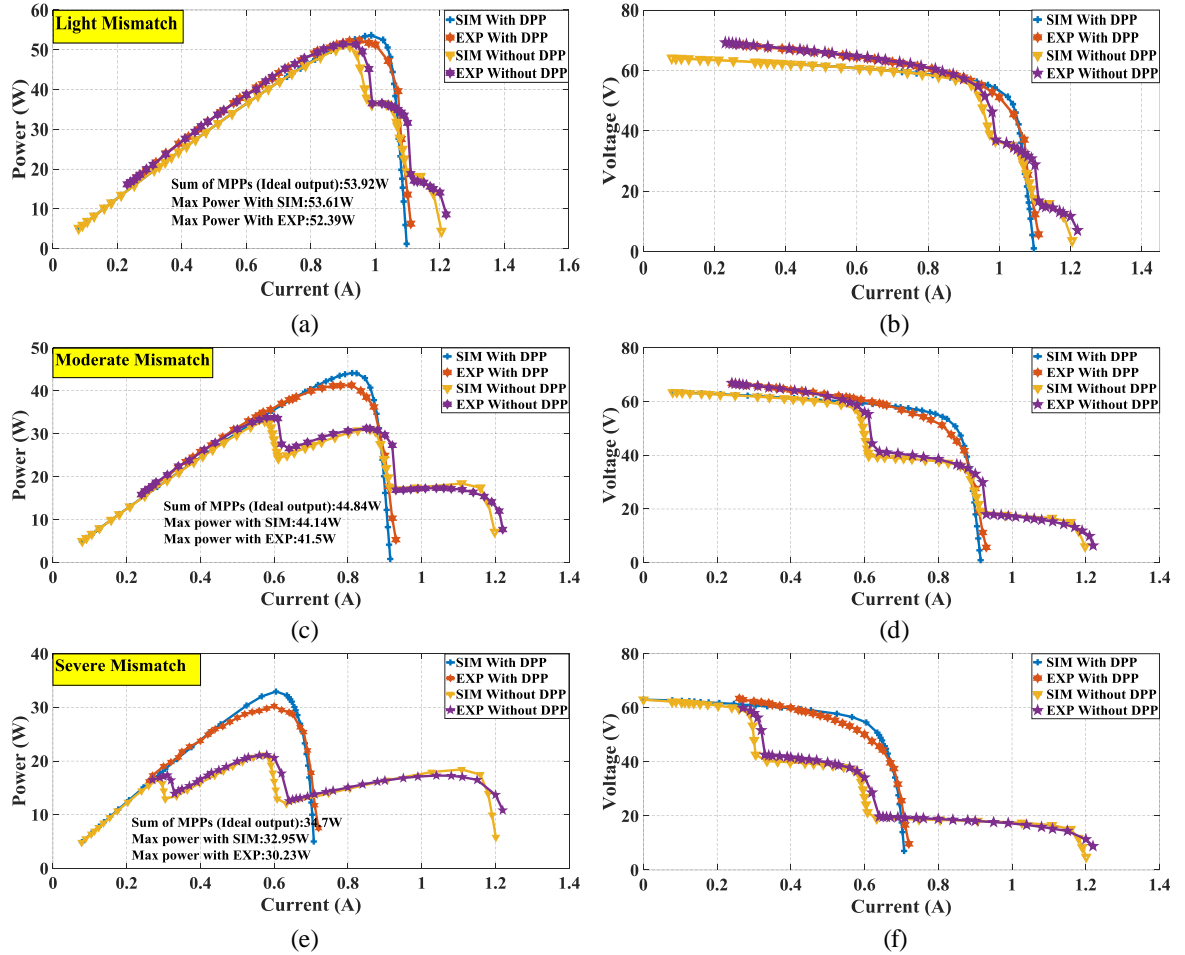


Fig. 21. Experimental results comparison: (a) P-I curve for slight mismatch condition (PV1: 100%, PV2: 90%, PV3: 80%); (b) V-I curve for slight mismatch condition (PV1: 100%, PV2: 90%, PV3: 80%); (c) P-I curve for moderate mismatch condition (PV1: 100%, PV2: 75%, PV3: 50%); (d) V-I curve for moderate mismatch condition (PV1: 100%, PV2: 75%, PV3: 50%); (e) P-I curve for severe mismatch condition (PV1: 100%, PV2: 50%, PV3: 25%); (f) V-I curve for severe mismatch condition (PV1: 100%, PV2: 50%, PV3: 25%).

The overall efficiency of the DPP system is measured under two operating conditions: no shading condition (bias current is 1.22A, 1.22A and 1.22A) and severe shading condition (bias current is 1.22A, 0.61A and 0.31A). The measured results under two conditions are illustrated in Table V, which indicates that an efficiency of 99.8% can be achieved without partial shading. Under this condition, all BFCs are bypassed and no power loss produced. With severe shading, the overall efficiency is 90% due to more mismatch power is processed by BFCs. Thus, additional power losses will be produced, and the system efficiency is affected. However, more output power is achieved by using the DPP structure, as illustrated in Table V.

TABLE V
MEASURED EFFICIENCY RESULTS UNDER TWO OPERATION CONDITIONS

Condition	No Shading	Severe Shading
Bias Current of each Substring	1.22 A 1.22A 1.22A	1.22A 0.61A 0.31A
Sum of MPPs (ideal output power)	60 W	33.5 W
Measure Maximum String Power	59.1 W	30.23 W
Power loss in BFCs	0.9 W	3.27 W
Efficiency	98.50%	90.23%

D. Transient Test

Transient performance is evaluated since totally three BFCs are used in the DPP structure. Similar to the transient simulation setting in Fig. 14, initially all submodules are supplied with the same current 1.22A. Then, at $t=1.5s$, the injected current to submodule 1 is reducing to 0.47A to emulate the partial shading. The measured current is: $i_{pri1} = -0.5A, I_{pri2} = I_{pri3} = 0.25A$ as illustrated in Fig. 22, which verifies the above theoretical steady-state analysis. The current redistribution dynamics among three branches are almost finished during the same period. The transient time is measured as 0.26s, which is higher than the simulation result of 0.06s considering the effect of parasitic effect, and single time delay. At $t=3.75s$, partial shading is setting disappeared, and the current for submodule 1 is increased to the normal bias current 1.22A. Fig. 22 shows that and the currents following through the BFCs are reduced to 0A. The current redistribution dynamics among three branches also shows good consistency.

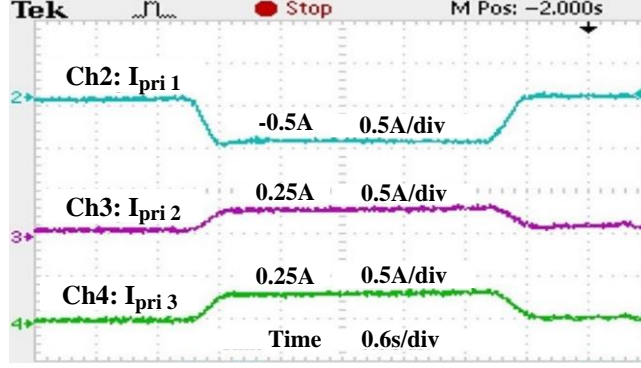


Fig. 22. Experimental transient response.

V. CONCLUSION

In this paper, we addressed the problem of submodule mismatch in partially-shaded PV modules by using bidirectional flyback-based isolated-port differential power-processing optimizers. Different to the PV-to-PV and PV-to-bus structure, the PV-to-isolated port structure is adopted since it processes the least power and shows potentially highest efficiency among different DPP structures. Furthermore, with this DPP structure, the voltage conversion ratio of the submodule DC-DC converters is close to unity, allowing low voltage components. The bidirectional flyback topology was selected since it can achieve voltage isolation, high efficiency for a wide range, and easy gate driver circuit design. The flyback converter designed to work in discontinuous conduction mode (DCM) for the slight mismatch condition and continuous conduction mode (CMM) for the severe mismatch condition to minimize the power loss. The voltage equalization with open-loop control is used to regulate the submodule flyback converter. The duty-ratio of submodule flyback converter is set as a fixed number with 0.5, and the frequency is 100 kHz. It's simple, easy-to-implement and well suited for low-cost integrated hardware scheme since it does not require additional voltage or current sensors. Besides, complex processing and communication between BFCs are removed. Both simulation and experimental results for a 72-cells PV module are provided. The measured efficiency with the isolated-port DPP structure was 98.50% with no shading, and 90.23% under severe shading condition. Under the moderate shading condition, the measured output power improvement was 26%. Under severe mismatch condition, the corresponding improvement was high up to 43.1%.

ACKNOWLEDGEMENTS

This research was supported by the University Research Development Fund (RDF-14-02-03), the State Key Laboratory of Power Transmission Equipment & System Security and New Technology (2007DA10512716414), the Jiangsu Science and Technology Programme (BK20161252), and the National Nature Science Foundation of China (51407145).

REFERENCE

- Bai, J., Y. Cao, Y. Hao, Z. Zhang, S. Liu and F. Cao., 2015. Characteristic output of PV systems under partial shading or mismatch conditions. *Solar Energy* **112**: 41-54.
- Bell, R. and R. C. N. Pilawa-Podgurski., 2015. Decoupled and Distributed Maximum Power Point Tracking of Series-Connected Photovoltaic Submodules Using Differential Power Processing. *IEEE Journal of Emerging and Selected Topics in Power Electronics* **3**(4): 881-891.
- Ben-Yaakov, S., A. Blumenfeld, A. Cervera and M. Evzelman., 2012. Design and evaluation of a modular resonant switched capacitors equalizer for PV panels. 2012 IEEE Energy Conversion Congress and Exposition (ECCE).
- Daliento, S., F. Di Napoli, P. Guerriero and V. d'Alessandro., 2016. A modified bypass circuit for improved hot spot reliability of solar panels subject to partial shading. *Solar Energy* **134**(Supplement C): 211-218.
- Du, Y. and D. D.-C. Lu., 2011. Battery-integrated boost converter utilizing distributed MPPT configuration for photovoltaic systems. *Solar Energy* **85**(9): 1992-2002.
- Eng, V. and C. Bunlaksananusorn., 2009. Modeling of a SEPIC converter operating in Discontinuous Conduction Mode. 2009 6th International Conference on Electrical Engineering/Electronics, Computer, Telecommunications and Information Technology.
- Eng, V., U. Pinsopon and C. Bunlaksananusorn., 2009. Modeling of a SEPIC converter operating in Continuous Conduction Mode. 2009 6th International Conference on Electrical Engineering/Electronics, Computer, Telecommunications and Information Technology.
- Khan, O. and W. Xiao., 2016. An Efficient Modeling Technique to Simulate and Control Submodule-Integrated PV System for Single-Phase Grid Connection. *IEEE Transactions on Sustainable Energy* **7**(1): 96-107.
- Khan, O. and W. Xiao., 2017. Review and qualitative analysis of submodule-level distributed power electronic solutions in PV power systems. *Renewable and Sustainable Energy Reviews* **76**: 516-528.
- Kim, K. A., G. S. Seo, B. H. Cho and P. T. Krein., 2016. Photovoltaic Hot-Spot Detection for Solar Panel Substrings Using AC Parameter Characterization. *IEEE Transactions on Power Electronics* **31**(2): 1121-1130.
- Kim, K. A., P. S. Shenoy and P. T. Krein., 2015. Converter Rating Analysis for Photovoltaic Differential Power Processing Systems. *IEEE Transactions on Power Electronics* **30**(4): 1987-1997.

- Lappalainen, K. and S. Valkealahti., 2017. Effects of PV array layout, electrical configuration and geographic orientation on mismatch losses caused by moving clouds. *Solar Energy* **144**(Supplement C): 548-555.
- Levron, Y., D. R. Clement, B. Choi, C. Olalla and D. Maksimovic., 2014. Control of Submodule Integrated Converters in the Isolated-Port Differential Power-Processing Photovoltaic Architecture. *IEEE Journal of Emerging and Selected Topics in Power Electronics* **2**(4): 821-832.
- Li, X., H. Wen, L. Jiang, Y. Hu and C. Zhao., 2016. An Improved Beta Method With Autoscaling Factor for Photovoltaic System. *IEEE Transactions on Industry Applications* **52**(5): 4281-4291.
- Mäki, A. and S. Valkealahti., 2012. Power Losses in Long String and Parallel-Connected Short Strings of Series-Connected Silicon-Based Photovoltaic Modules Due to Partial Shading Conditions. *IEEE Transactions on Energy Conversion* **27**(1): 173-183.
- Mai, T. D., S. De Breucker, K. Baert and J. Driesen., 2017. Reconfigurable emulator for photovoltaic modules under static partial shading conditions. *Solar Energy* **141**: 256-265.
- Olalla, C., D. Clement, M. Rodriguez and D. Maksimovic., 2013. Architectures and Control of Submodule Integrated DC-DC Converters for Photovoltaic Applications. *IEEE Transactions on Power Electronics* **28**(6): 2980-2997.
- Qin, S., C. B. Barth and R. C. N. Pilawa-Podgurski., 2016. Enhancing Microinverter Energy Capture With Submodule Differential Power Processing. *IEEE Transactions on Power Electronics* **31**(5): 3575-3585.
- Qin, S., S. T. Cady, A. D. Domínguez-García and R. C. N. Pilawa-Podgurski., 2015. A Distributed Approach to Maximum Power Point Tracking for Photovoltaic Submodule Differential Power Processing. *IEEE Transactions on Power Electronics* **30**(4): 2024-2040.
- Radjai, T., L. Rahmani, S. Mekhilef and J. P. Gaubert., 2014. Implementation of a modified incremental conductance MPPT algorithm with direct control based on a fuzzy duty cycle change estimator using dSPACE. *Solar Energy* **110**: 325-337.
- Rezk, H. and A. M. Eltamaly., 2015. A comprehensive comparison of different MPPT techniques for photovoltaic systems. *Solar Energy* **112**: 1-11.
- Schaefer, C., K. Kesarwani and J. T. Stauth., 2013. A coupled-inductor multi-level ladder converter for sub-module PV power management. 2013 Twenty-Eighth Annual IEEE Applied Power Electronics Conference and Exposition (APEC).
- Shenoy, P. S., K. A. Kim, B. B. Johnson and P. T. Krein., 2013. Differential Power Processing for Increased Energy Production and Reliability of Photovoltaic Systems. *IEEE Transactions on Power Electronics* **28**(6): 2968-2979.
- Solórzano, J. and M. A. Egidio., 2014. Hot-spot mitigation in PV arrays with distributed MPPT (DMPPT). *Solar Energy* **101**: 131-137.
- Tey, K. S. and S. Mekhilef., 2014. Modified incremental conductance MPPT algorithm to mitigate inaccurate responses under fast-changing solar irradiation level. *Solar Energy* **101**: 333-342.

- Uno, M. and A. Kukita., 2015. Current sensorless single-switch voltage equalizer using multi-stacked buck-boost converters for photovoltaic modules under partial shading. 2015 9th International Conference on Power Electronics and ECCE Asia (ICPE-ECCE Asia).
- Villa, L. F. L., T. P. Ho, J. C. Crebier and B. Raison., 2013. A Power Electronics Equalizer Application for Partially Shaded Photovoltaic Modules. IEEE Transactions on Industrial Electronics **60**(3): 1179-1190.
- Zhou, H., J. Zhao and Y. Han., 2015. PV Balancers: Concept, Architectures, and Realization. IEEE Transactions on Power Electronics **30**(7): 3479-3487.